

See discussions, stats, and author profiles for this publication at: <https://www.researchgate.net/publication/231644424>

Exploration of Half Metallicity in Edge-Modified Graphene Nanoribbons

ARTICLE *in* THE JOURNAL OF PHYSICAL CHEMISTRY C · FEBRUARY 2010

Impact Factor: 4.77 · DOI: 10.1021/jp100027w

CITATIONS

68

READS

23

3 AUTHORS:



Menghao Wu

Massachusetts Institute of Technology

20 PUBLICATIONS 374 CITATIONS

[SEE PROFILE](#)



Xiaojun Wu

University of Science and Technology of C...

114 PUBLICATIONS 2,264 CITATIONS

[SEE PROFILE](#)



Zeng Cheng

University of Science and Technology of C...

378 PUBLICATIONS 6,649 CITATIONS

[SEE PROFILE](#)

Exploration of Half Metallicity in Edge-Modified Graphene Nanoribbons

Menghao Wu,^{†,‡} Xiaojun Wu,[†] and Xiao Cheng Zeng^{*,†,‡}

Department of Chemistry, Department of Physics and Astronomy, University of Nebraska-Lincoln, Lincoln, Nebraska, 68588

Received: January 2, 2010

A systematic study of various edge modified graphene nanoribbons (GNRs) have been performed using a density functional theory method. Particular attention is placed on the possibility of achieving half-metallicity in the graphene nanostructures. Six chemical functional groups, namely, OH, NH₂, N(CH₃)₂, SO₂, NO₂, and CN, are considered for the edge modification. Density functional theory (DFT) calculations with Perdew–Burke–Ernzerhof (PBE) functional suggest that half-metallicity can be realized in zigzag-edged GNRs (ZGNRs) when one edge of the graphene is fully decorated with the OH group while the other edge is decorated with either NO₂ or SO₂ functional group. Moreover, DFT/PBE calculations suggest that the half-metallicity can be realized via modification of one edge with hybrid X groups (X = SO₂, NO₂, or CN) and hydrogen (H) atoms. Two mechanisms can lead to half-metallicity in ZGNRs, (1) chemical-potential mechanism, that is, to create a difference in chemical potential between the two edges by decorating one edge with electron-donating groups and another with electron-accepting groups, which can lead to spin-polarized states in the electronic band gap, and (2) impurity-state mechanism, that is, to introduce a spin-polarized impurity state at the Fermi level through partial modification of one edge with isolated SO₂ groups. More specifically, for a narrow ZGNR, both DFT/PBE and DFT/hybrid Heyd–Scuseria–Ernzerhof calculations show that the impurity-state mechanism can be realized with hybrid SO₂ and H decorated edge. To our knowledge, the second mechanism has not been reported in the literature. A major advantage of the impurity-state mechanism is its insensitivity to the chemical potential difference between the two edges of a ZGNR. As such, the opposing edge to the SO₂-decorated edge can be decorated by a variety of functional groups (e.g., F, H, or OH) to meet the needs for nanoelectronic applications by design.

Introduction

Graphene, a single layer of graphite, has attracted considerable research interests owing to its novel physical properties, such as massless Dirac fermion behavior,^{1–5} room-temperature quantum hall effect^{6,7} and high mobility.⁸ The two-dimensional (2D) graphene sheet itself is a semimetal. However, when the 2D sheet is cut into long rectangle slices, namely, the graphene nanoribbons (GNRs), they can become semiconductors with the band gap depending on the width of GNRs as well as the crystallographic orientation of cutting edges. Hence, GNRs possess tunable electronic properties, rendering GNR-based nanoelectronic devices viable.^{9–20}

Besides width-dependent semiconducting properties, previous theoretical studies have also revealed that zigzag-edged GNRs (ZGNRs) can be converted into half metals by either applying an external electric field or through chemical modification of the edges. Half metals hold the promise for spintronic applications^{18,21–27} as the electric current is fully spin polarized when going through half metals because one electron spin channel is insulating while the other is metallic. Son et al. were the first to show that half-metallicity can be achieved in a ZGNR by applying a strong in-plane transverse electric field.²⁴ The applied electric field induces an electrostatic-potential difference between the two edges of a ZGNR, leading to a spin-polarized band crossing of the Fermi level. An important physical insight attained from this study is that the generation of an electrostatic

potential difference between the two edges of a ZGNR is a prerequisite for achieving half metallicity. Inspired by this study, Kan et al. suggested an alternative way to obtain GNR-based half metals. They showed that if the two edges of a ZGNR can be decorated with NO₂ and CH₃ chemical function groups, respectively, the ZGNR can be converted to a half metal²⁵ because the chemical modification elevates certain spin-polarized bands crossing the Fermi level.

Nevertheless, not all heterogeneous edge modification could convert a ZGNR into a half metal. In this article, we present a systematic study of electronic structures of ZGNRs whose edges are decorated with various chemical functional groups, including OH, NH₂, N(CH₃)₂, SO₂, NO₂, and CN. Our study suggests that OH can be a promising functional group for achieving half-metallicity in ZGNRs. For the opposing edge, there are some degrees of flexibility in choosing a chemical functional group, or multiple functional groups with hybrid edge-site decoration. Alternatively, a ZGNR-based half metal can be possibly produced by introducing a spin-polarized impurity state at the Fermi level through hybrid modification of one edge with isolated SO₂ groups.

Theoretical Methods, Model Systems, and Benchmark Test

The density function theory (DFT) calculations were carried out using the Vienna Ab initio Simulation Package (VASP).^{28–30} The projector augmented wave (PAW) potentials for the core and the generalized gradient approximation (GGA) in the Perdew–Burke–Ernzerhof (PBE) form³¹ for the exchange-correlation functional are applied. For geometric optimization,

* To whom correspondence should be addressed.

[†] Department of Chemistry.

[‡] Department of Physics and Astronomy.

TABLE 1: Measured Band Gaps (In Bold) of a 2.3 nm Wide Predominantly Zigzag GNR and a 3.3 nm Wide Predominantly Zigzag GNR, Compared to Calculated Band Gaps Using PBE (GGA) and Hybrid HSE Functional, Respectively, of a Perfect 2.3 nm Wide 12-ZGNR and a Perfect 3.3 nm Wide 16-ZGNR with Their Edges Passivated by H

	H/H-12-ZGNR	H/H-16-ZGNR
experiment ³⁷	~0.14 eV	~0.12 eV
PBE calc	0.44 eV	0.29 eV
HSE calc	1.0 eV	0.82 eV

a tetrahedral supercell with dimension $30 \times 16 \times 2c \text{ \AA}^3$ with one periodic length, or $30 \times 10 \times 2c \text{ \AA}^3$ with two periodic lengths, or $30 \times 10 \times 3c \text{ \AA}^3$ with three periodic lengths was opted, where c is the length of a unit cell along the ribbon direction. The distance between the GNR and its nearest images is greater than 10 Å. The kinetic energy cutoff was set to be 500 eV. For band-structure calculation, the Brillouin zone was sampled by $1 \times 1 \times 20$ k points using the Monkhorst-Pack scheme.³²

In addition to PBE functional, we also computed electronic structures of some systems using the screened exchange hybrid Heyd–Scuseria–Ernzerhof (HSE) functional.^{33,34} It is known that DFT within either local-density approximation (LDA) or GGA generally underestimates band gaps of bulk semiconductors and insulators while hybrid functionals such as HSE typically gives more accurate results of band gaps.^{33,34} For quasi-one-dimensional semiconducting systems such as armchair GNRs, previous theoretical studies have also shown that the LDA significantly underestimates the band gaps in comparison with more accurate GW method.^{35,36} For zigzag GNRs, we computed band gaps of two perfect ZGNR systems, (1) a 2.3 nm wide 12-ZGNR and a 3.3 nm wide 16-ZGNR with edge passivation by hydrogen, using both PBE and HSE functionals. We chose the two ZGNR systems so that we can compare with a recent measurement of the band gaps of two predominantly ZGNR systems; one is 2.3 nm wide and another is 3.3 nm wide.³⁷ Unexpectedly, the PBE calculation shows that the perfect 12-ZGNR and 16-ZGNR exhibit larger band gaps than those of imperfect ones (see Table 1). Note that both experimental samples have mixed armchair and unknown edges. A previous theoretic study indicates that mixed edge structures can significantly affect the band gaps of GNRs.¹⁹ Hence, a more reliable comparison between DFT calculations and experimental measurements of band gaps of ZGNRs must await fabrication of near-perfect ZGNRs.

Results and Discussions

Hereafter, we use the notation n-ZGNR to describe a ZGNR with n zigzag carbon chains. Especially, we consider the 8-ZGNR as a prototype model system. As mentioned previously, the use of heterogeneous chemical function groups for edge decoration can induce a potential difference between two edges of a ZGNR. In general, both the conduction and valence band edges in one spin channel are shifted with the edge modification. If the shift causes a band crossing through the Fermi level, half-metallicity is achieved. One way to generate sufficiently large potential difference between the two edges is to decorate one edge with electron donating groups such as OH, NH₂, or N(CH₃)₂, and another with electron accepting groups, such as NO₂, SO₂, and CN. Previously, Kan et al. showed that NO₂ can be an effective electron-accepting group for edge decoration.²⁵ They predicted that when coupled with the CH₃ groups

at the opposing edge, half-metallicity can be induced.²⁵ On the electron-donating group, however, they found that when one edge is fully decorated by three-atom groups such as NH₂ the strong repulsive (steric) interactions among nearest-neighbor NH₂ groups can cause notable local strain near the graphene edge. To avoid large local strain, we considered a hybrid edge decoration with both NH₂ functional groups and hydrogen atoms on every other edge sites.

Homogeneous Edge Decoration. First, we show electronic properties of an 8-ZGNR modified with the same type of functional groups at both edges (i.e., homogeneous edge decoration). Figure 1 display the optimized geometric structures, the computed band structures (using PBE functional), as well as the partial density of states (PDOS) of the chemical groups and carbon atoms at the edges, for several chemically modified 8-ZGNRs. Note that a pristine 8-ZGNR is a semiconductor with a narrow direct band gap of ~0.45 eV. Figure 1a shows that the OH-decorated 8-ZGNR has a similar profile of electronic band structures as the pristine 8-ZGNR, but the band gap is 0.17 eV less than that of the pristine 8-ZGNR. As shown in Figure 1c,d, the three-atom NO₂ or SO₂ functional groups induce local out-of-plane structural distortions at each edge sites due to strong repulsive (steric) interactions among nearest-neighbor functional groups. In addition, the optimized supercell length along the ribbon direction increases from 4.93 Å (for the pristine 8-ZGNR) to 4.97 Å. The edge modified 8-ZGNR by either NO₂ or SO₂ groups is still a semiconductor but with an indirect band gap of 0.26 eV. The plotted PDOS in Figure 1a–d show that the states near the Fermi level are mainly contributed by C atoms at the edges rather than the functional groups. In contrast, the CN decorated 8-ZGNR is a semimetal because of the appearance of certain impurity states that cross the Fermi level. These impurity states are mainly induced by the CN groups.

The average substitution energy per functional group X for the replacement of hydrogen atoms H by functional groups X at the two edges is defined as

$$E_s = (E(X-ZGNR) + mE(H) - E(H-ZGNR) - mE(X))/m$$

where $E(\text{system})$ is the total energy of the system per supercell, X denotes the functional group (OH, SO₂, NO₂, or CN), H is the hydrogen atom, and m is the number of functional groups per supercell. The calculated average substitution energies per functional group are –0.19, 3.55, 2.75, and –1.37 eV for OH, SO₂, NO₂, and CN group, respectively. The positive E_s in the case of NO₂ or SO₂ indicates the corresponding edge decoration costs more energy compared to the edge decoration by hydrogen atoms.

Heterogeneous Edge Decoration. (a) One Edge Fully Decorated by OH groups. Here, we show computed electronic properties of an 8-ZGNR decorated by OH functional groups at one edge and by X groups (X = SO₂, NO₂, CN) at the other edge. The edge decorated 8-ZGNRs are labeled as OH/X-8-ZGNR. The optimized structures and computed electronic band structures (based on PBE functional) of OH-X-8-ZGNR are shown in Figure 2. The PBE calculations suggest that the OH/SO₂-8-ZGNR and OH/NO₂-8-ZGNR are half metallic, as the conduction and valence band edges in one spin channel cross the Fermi level. In the other spin channel there exists an indirect band gap of about 0.5 eV. Again, the relatively larger three-atom NO₂ or SO₂ functional groups induce out-of-plane structural distortions at each edge sites. In

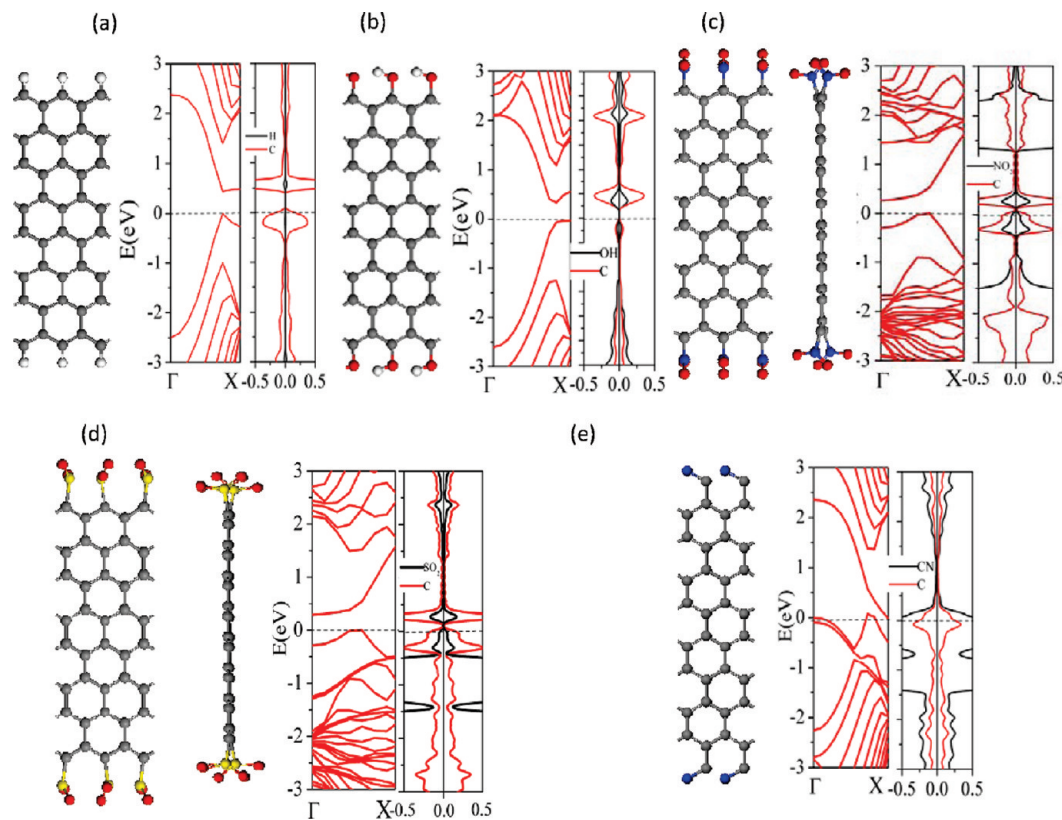


Figure 1. Geometric structures, electronic band structures, and PDOS of functional groups and carbon atoms at the edges of 8-ZGNRs. The two edges are uniformly decorated by (a) H, (b) OH, (c) NO₂, (d) SO₂, and (e) CN groups. Small gray, white, blue, yellow, and red spheres denote carbon, hydrogen, nitrogen, sulfur, and oxygen atoms. Out-of-plane structural distortions at the two edges can be seen in side view of the structure in (c,d). The optimized value of unit-cell length c in the ribbon direction is (a) 2.465 Å, (b) 2.465 Å, (c) 2.485 Å, (d) 2.485 Å, and (e) 2.465 Å, respectively. In the corresponding PDOS plots, positive region represents the spin-up channel and negative region represents the spin-down channel. The Fermi level is denoted by a horizontal black dashed line.

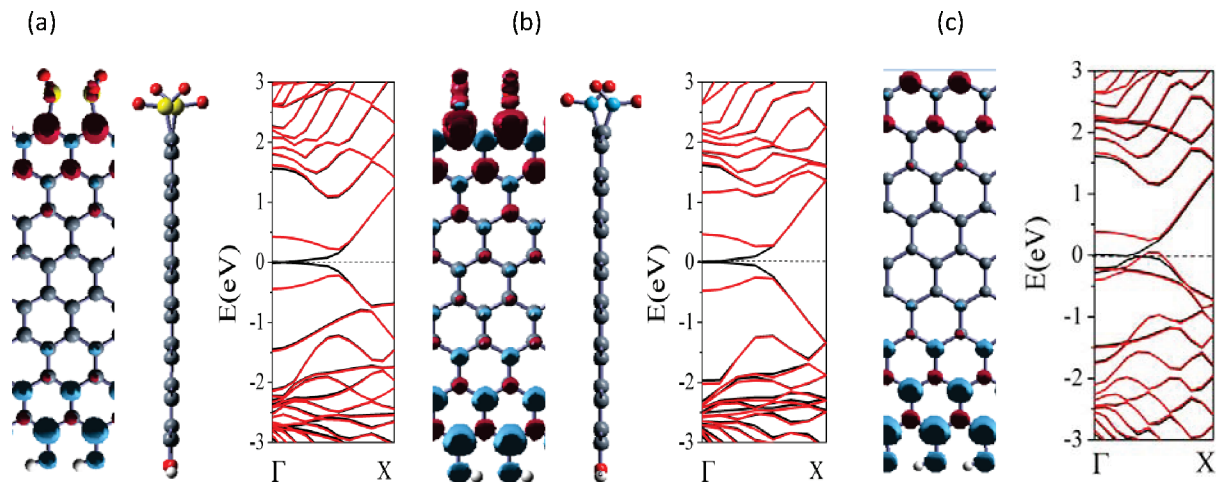


Figure 2. Geometric structures, spin densities, and electronic band structures (PBE calculation) of 8-ZGNRs with their two edges (top/bottom edges) decorated by (a) SO₂/OH groups, (b) NO₂/OH groups, or (c) CN/OH groups. The S-S distance is 2.085 Å in (a). The larger cyan and maroon spheres represent local spin-up and spin-down density, respectively. In the corresponding band structure plots (a-c), black lines represent the spin-up channel and red lines represent the spin-down channel. The Fermi level is denoted by a horizontal black dashed line.

contrast, the OH/CN-8ZGNR is predicted to be metallic, similar to the homogeneous edge decoration of the 8-ZGNR with all CN groups.

In addition, we performed calculations for the same OH/SO₂-8-ZGNR and OH/NO₂-8-ZGNR systems but using a LDA functional and the hybrid HSE functional, respectively. Calculated band structures are shown in the Supporting Information-Figure S1. It can be seen that LDA also predicts that both systems are half metallic, consistent with PBE calculations.

However, the HSE functional predicts that both systems are spin-polarized semiconductors because the HSE functional predicts larger band gaps for both spin channels.

Heterogeneous Edge Decoration. (b) One Edge Fully Decorated by Hybrid X and H. One way to alleviate the strong steric repulsion between nearest-neighbor functional groups is to reduce the fraction of the three-atom functional groups (such as SO₂, NO₂) at the edges, for example, by replacing every other SO₂ or NO₂ group with a smaller hydrogen atom for the edge

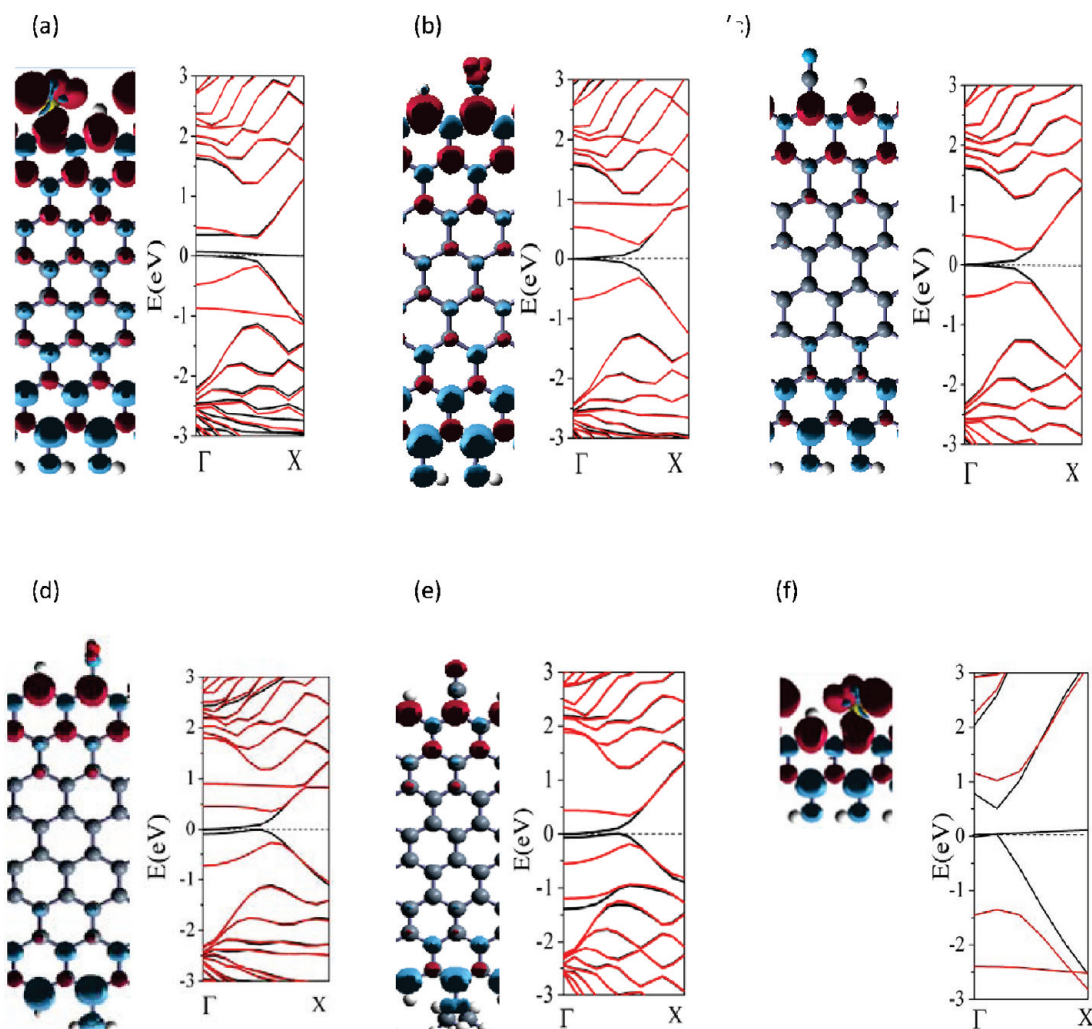


Figure 3. Geometric structures, spin densities, and band structures (PBE calculations) of 8-ZGNRs with two edges (top/bottom edges) decorated by (a) SO₂+H/OH, (b) NO₂+H/OH, (c) CN+H/OH, (d) NO₂+H/NH₂+H, or (e) CN+H/N(CH₃)₂+H hybrid groups and atoms. The larger cyan and maroon spheres represent local spin-up and spin-down density, respectively. (f) Geometric structure, spin density, and band structure (HSE calculations) of a 2-ZGNR with two edges decorated by SO₂+H/OH.

decoration (see Figure 3). Clearly, the replacement of a larger functional group by a much smaller H atom completely removes the local out-of-plane structural distortion occurred in fully decorated ZGNRs. The calculated average substitution energies are 3.32 and 2.25 eV for SO₂ and NO₂, respectively, for hybrid edge decoration with H. Both substitution energy values are less than those in fully decorated ZGNRs, suggesting that the removal of local structural distortions via introducing H atoms actually increases the stability of the system.

The hybrid decoration with H and X (= SO₂ or CN) at one edge, labeled as H+X/OH-8-ZGNR, gives rise some new features in the electronic structure. For example, the PBE calculations suggest that CN+H/OH-8-ZGNR is possibly half metallic (see Figure 3c) even though the CN/OH-8-ZGNR is metallic (Figure 2c). More interestingly, for the H+SO₂/OH-8-ZGNR, the computed electronic structure (Figure 3a) indicates the ribbon is a different type of half metal from the SO₂/OH-8-ZGNR (Figure 2a). For the latter, the spin-up channel shows a direct zero band gap, whereas for H+SO₂/OH-8-ZGNR the spin-up channel shows an indirect zero band gap. In fact, for H+SO₂/OH-8-ZGNR, an impurity state is induced at the Fermi level, resulting in the new type of half metal although the SO₂/OH-8ZGNR has a similar electronic structure as NO₂+H/OH-8-ZGNR (see Figure 2b).

Besides the electron-accepting groups, the electron-donating groups, for example, OH, can be also replaced by hybrid NH₂

groups plus H atoms, or by N(CH₃)₂ groups plus H atoms (see Figure 3d,e). For example, when the OH groups in H+NO₂/OH-8-ZGNR or H+CN/OH-8-ZGNR are fully replaced by NH₂+H or N(CH₃)₂+H groups, the PBE calculations suggest that the ribbons are possibly half metallic. However, instead of direct zero band gap in the spin-up channel, both edge modified ribbons exhibit indirect zero band gap in the spin-up channel (see Figure 3d,e).

The three distinct zero band gap features in the electronic structures can be attributed to two fundamental mechanisms for potentially achieving half metallicity. The first mechanism is already well known in which the band gap closing in one spin channel stems from the chemical potential difference between two edges. The zero band gap can be either direct, as shown in Figures 2a,b and 3b,c, or indirect, as shown in Figure 3d,e. The second mechanism, to our knowledge, appears to be a new one. As shown in Figure 3a, an impurity state is induced at the Fermi level in one spin channel, resulting in the zero band gap. More interestingly, for an OH/SO₂ decorated GNR system with smaller width ($n = 2$) than OH/SO₂-8-ZGNR, even the hybrid HSE calculation predicts the onset of half metallicity (see Figure 3f), consistent with the PBE calculation result. Hence, this ZGNR system is predicted to be the most likely to exhibit type-2 half metallicity.

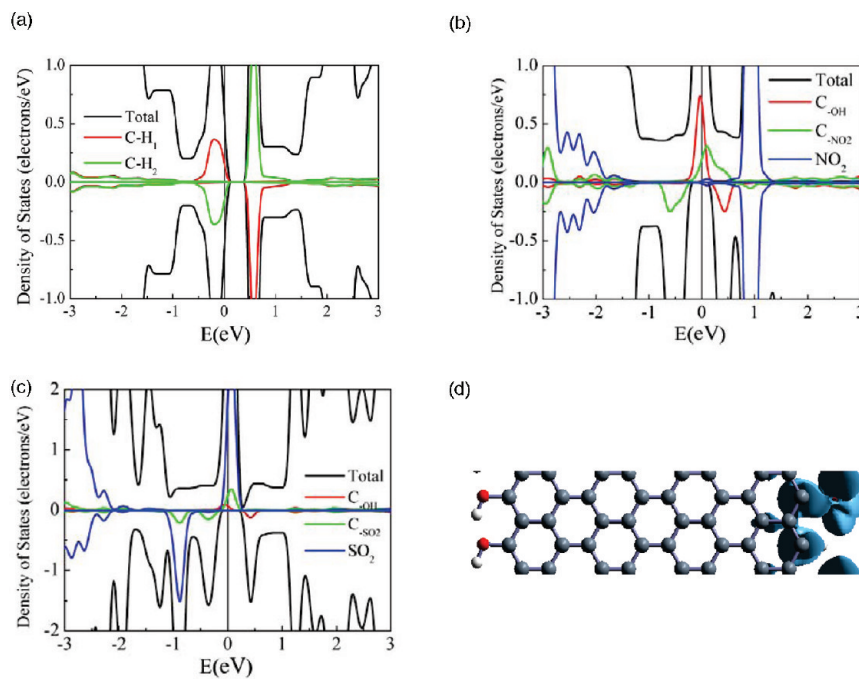


Figure 4. Spin-polarized partial density of states of (a) C-H atoms at the edges and all atoms in the supercell for H/H-8-ZGNR; (b) C-NO₂, C-OH atoms at the edges, NO₂ group, and all atoms in the supercell for H+NO₂/OH-8-ZGNR; and (c) C-SO₂, C-OH atoms at the edges, SO₂ group, and all atoms in the supercell for H+SO₂/OH-8-ZGNR. Positive density region represents the spin-up channel and negative region represents the spin-down channel. The Fermi level is denoted by a vertical black line at 0 eV. (d) The density distribution of the impurity band (i.e., the lowest unoccupied band) of H+SO₂/OH-8-ZGNR.

The difference in the two mechanisms is also reflected in the spin charge density distribution. In the first mechanism, the spin charge density is mainly contributed by carbon atoms at the edges, whereas in the second, the spin charge density is contributed by both the SO₂ groups and the carbon atoms at the edges (see Figure 3a,f).

To further illustrate the difference between the two mechanisms, the projected density of states (PDOS) on the functional groups and carbon atoms at the edges of a pure 8-ZGNR, H+NO₂/OH-8-ZGNR, and H+SO₂/OH-8-ZGNR are plotted in Figure 4, respectively. For the pure 8-ZGNR (Figure 4a), the carbon atoms at the edges contribute separated conduction and valence PDOS peaks near the Fermi level. These peaks show the mirror symmetry with respect to the horizontal axis. Hence, the pure ZGNR is a spin-nonpolarized semiconductor. For H+NO₂/OH-8-ZGNR (Figure 4b), the PDOS peaks (near the Fermi level) contributed by the carbon atoms bonded to NO₂ (C-NO₂) are shifted downward with respect to the Fermi level, while those peaks contributed by the carbon atoms bonded to OH (C-OH) are shifted upward. Both shifts are due to the chemical potential difference between the two edges.²⁶ In this case, no PDOS peak near the Fermi level is contributed by NO₂ and OH groups. On the other hand, for H+SO₂/OH-8-ZGNR (Figure 4c), the PDOS peaks (near the Fermi level) contributed by C-OH are shifted upward, similar to those for H-NO₂/OH-8-ZGNR, but the PDOS peaks contributed by C-SO₂ retain their positions in energy. Instead, a new impurity state in one spin channel emerges slightly above the Fermi level. Hence, this impurity band is the lowest unoccupied band (LUB). The density distribution of the impurity band (i.e., the LUB) is plotted in Figure 4d, which shows that the profile of the impurity state at the γ-point is mainly contributed by the SO₂ functional groups. In summary, the PDOS analysis suggests that the impurity state mainly originates from a coupling among those carbon atoms at the edge with SO₂ functional groups.

Heterogeneous Edge Decoration. (c) One Edge Fully Decorated by SO₂ and H at Various Molecular Ratio. It is expected that the exact 1:1 ratio of SO₂ vs H is difficult to realize in experiments. Hence we have also investigated electronic structures of H+SO₂/OH-8-ZGNR with different molecular-number ratios of H/SO₂. The optimized geometric structures, computed band structures, and DOS of H+SO₂/OH-8-ZGNR with 1:2 or 2:1 ratio of H/SO₂, respectively, are shown in Figure 5. The average substitution energy of the SO₂ functional groups in place of H atoms, and the C–S bond lengths at different H/SO₂ ratios are summarized in Table 2. It is found that when the H/SO₂ ratio = 2:1 and when every two H atoms are located between two SO₂ functional groups, as shown in Figure 5a, the average substitution energy per SO₂ in H+SO₂/OH-8-ZGNR is the second lowest while the C–S bond length is the longest. More interestingly, as shown in Figure 5b, when two side-by-side SO₂ functional groups form a pair and a single H atom is located between the two SO₂ pairs, no out-of-plane structural distortion of S atoms was observed in this case. This is because the two S atoms adjust their in-plane position (the S–S distance is 2.262 Å, compared to 2.085 Å in Figure 2a) to mitigate the strong steric interaction. Indeed, as shown in Table 2, the substitution energy per SO₂ in this case is the lowest, indicating that this configuration is the most stable among the four.

Again, the calculated band structures (based on PBE functional) suggest that all H+SO₂/OH-8-ZGNR with the H/SO₂ ratio between 1:2 and 2:1 are possibly half metallic. The calculated band gaps in the semiconducting spin channel are 0.3 and 0.5 eV for H/SO₂ ratio = 2:1 and 1:2, respectively. When the H/SO₂ ratio is 2:1, an impurity state is introduced at the Fermi level and a large spin charge density is distributed over the SO₂ functional groups, as in the case of H/SO₂ ratio = 1:1. On the other hand, when the H/SO₂ ratio is 1:2, two side-by-side SO₂ functional groups form a pair, and the two neighboring S atoms form a weak S–S bond with a bond length

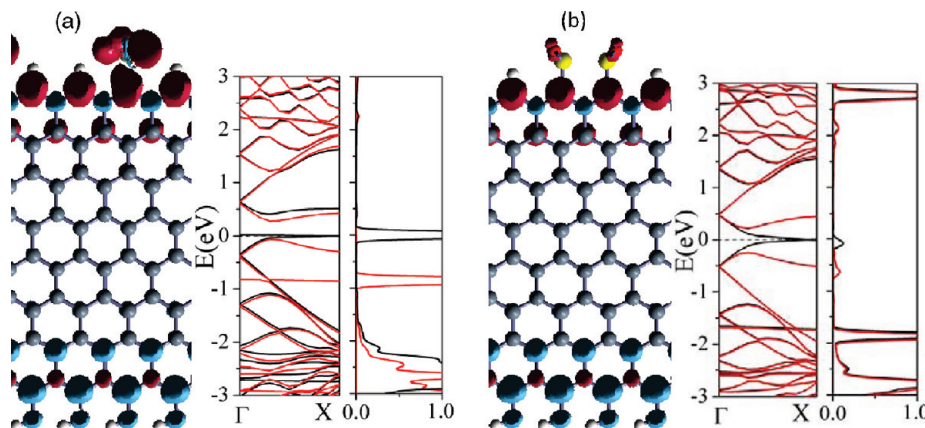


Figure 5. Spin densities, band structures, and the PDOS due to SO_2 for $\text{H}+\text{SO}_2/\text{OH}-8\text{-ZGNR}$ with the H/SO_2 ratio at one edge being (a) 2:1 and (b) 1:2. The S–S distance is 2.262 Å in (b). In the corresponding band structure and PDOS plots, black lines represent the spin-up channel and red lines represent the spin-down channel. The Fermi level is denoted by a horizontal black dashed line.

TABLE 2: The C–S Bond Lengths and Average Substitution Energies of SO_2 at Different Ratios of H/SO_2 in $\text{H}+\text{SO}_2/\text{OH}-8\text{-ZGNR}$

H/SO_2 ratio	0 (SO_2 only)	1:2	1:1	2:1
C–S bond length (Å)	1.786	1.778	1.836	1.839
substitution energy E_s (eV)	3.55	2.71	3.32	3.03

~2.262 Å, shorter than the distance 2.46 Å between two neighboring carbon atoms at the edge. The deformation density charge distribution further confirms that there is some covalent bonding character between two neighboring S atoms (Supporting

Information, Figure S2). In this case, the system could still be half metallic but the mechanism is chemical-potential-based rather than impurity-band-based as the band structures exhibits similar profiles as those of $\text{OH}/\text{SO}_2-8\text{-ZGNR}$ and the spin charge density mainly distribute over the carbon atoms at the edges (see Figure 5b). It is remarkable that a change from one mechanism to the other for achieving half metallicity can be controlled by changing the H/SO_2 ratio at one edge. These results also suggest that the impurity band is likely due to a lone pair of electrons of S atom in the SO_2 functional group. When two side-by-side SO_2 functional groups form a pair, the

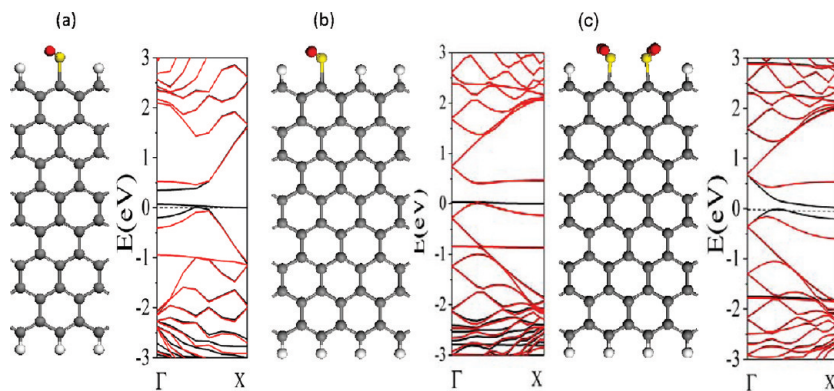


Figure 6. Geometric and band structures of $\text{H}+\text{SO}_2/\text{H}-8\text{-ZGNR}$ with the H/SO_2 ratio at one edge being (a) 1:1, (b) 2:1, and (c) 1:2.

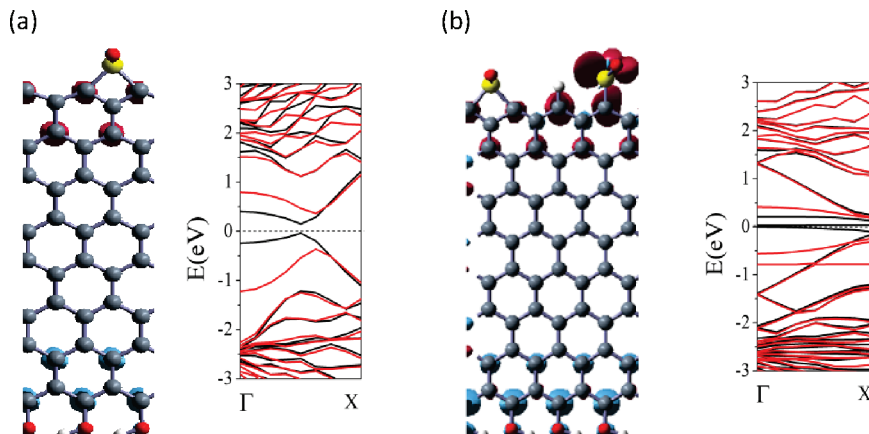


Figure 7. Spin densities, geometric structures, and band structures of the $\text{H}+\text{SO}_2/\text{OH}-8\text{-ZGNR}$ systems with (a) every H atom in between SO_2 groups and (b) every other H atom in between SO_2 groups being removed. In the band structure plots, the black lines represent the spin-up channel and red lines represent the spin-down channel. The Fermi level is denoted by a horizontal black dashed line.

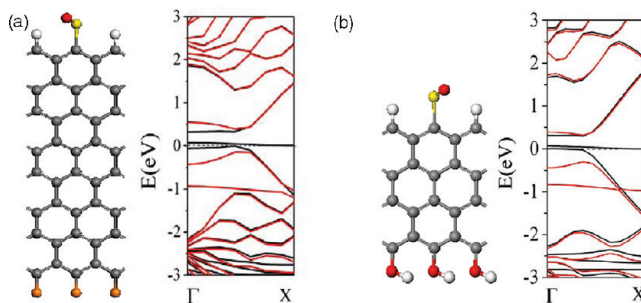


Figure 8. Geometric structures and band structures of (a) $\text{H}+\text{SO}_2/\text{F}-8\text{-ZGNR}$ where one edge is fully decorated by F atoms and of (b) $\text{H}+\text{SO}_2/\text{OH}-4\text{-ZGNR}$. Small gray, white, orange, yellow, and red spheres denote carbon, hydrogen, fluorine, sulfur, and oxygen atoms, respectively.

formation of a weak S–S bond consumes the lone pair electrons, hence removes the impurity band.

On the other hand, when many two SO_2 functional groups form pairs, they tend to generate sufficiently large chemical potential (together with OH functional groups at the opposing edge) between the two edges (the chemical-potential mechanism). To confirm this physical picture, we have performed a test calculation for an 8-ZGNR with one edge decorated by SO_2 functional groups and H atoms, and with the other edge fully decorated by H atoms (nonelectron-donating). As shown in Figure 6a,b, indeed the impurity states are introduced in the $\text{H}+\text{SO}_2/\text{H}-8\text{-ZGNRs}$ with the H/SO_2 ratio at one edge being 1:1 or 2:1; that is, the system may still be half metallic and the impurity-state mechanism prevails. However, when the H/SO_2 ratio is 1:2, the system is surely not half metallic but becomes a spin-polarized semiconductor, as shown in Figure 6c. This is because the chemical potential difference between the two edges is greatly reduced due to the replacement of OH by H.

The results above imply that the inclusion of hydrogen between SO_2 groups at one edge also plays an important role in potentially achieving half-metallicity. A question arises as to whether this system can still be converted to a half metal if the hydrogen atoms between the SO_2 functional groups are all removed. A test calculation shows that in the absence of H in between SO_2 groups, every SO_2 will be relocated and bind with two neighbor edge C atoms (Figure 7a). As such, the impurity state no longer exists. Hence, hydrogen atoms place the role of “separators” that prevent the SO_2 functional groups to be relocated to the middle of two edge C atoms. Nevertheless, if only a small portion of H atoms, for example, every other H atoms between SO_2 groups are removed, the impurity state still arises and the system could be converted to a half metal (Figure 7b).

A major advantage of the impurity-state mechanism is that the predicted half-metallicity is insensitive to the potential difference between the two edges of a ZGNR. As such, with isolated SO_2 functional groups at one edge, the other edge of ZGNR can be decorated by a variety of functional groups such as F, H, or OH (or even without edge decoration, as shown in Supporting Information, Figure S3), to meet the specific needs for nanoelectronic applications. For example, as shown in Figure 8a, the use of either H atoms as in $\text{H}+\text{SO}_2/\text{H}-8\text{-ZGNR}$ or F atoms as in $\text{H}+\text{SO}_2/\text{F}-8\text{-ZGNR}$ for decorating the opposing edge does not affect the underlying half-metallic property of the ribbon.

Another merit of the impurity-state mechanism is that the predicted half-metallicity is insensitive to the width of nanoribbons. As shown in Figure 8b, $\text{H}+\text{SO}_2/\text{OH}-4\text{-ZGNR}$ has a width of $n = 4$, and yet it can still be half metallic. In stark

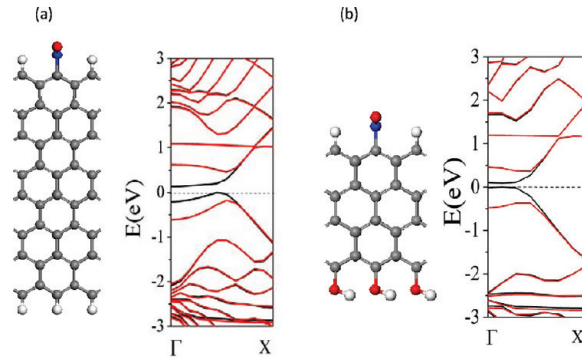


Figure 9. Geometric structures and band structures of (a) $\text{H}+\text{NO}_2/\text{H}-8\text{-ZGNR}$ where one edge is fully decorated by H atoms and of (b) $\text{H}+\text{NO}_2/\text{OH}-4\text{-ZGNR}$.

contrast, the half metallicity achieved via the chemical-potential mechanism can be quite sensitive to the selected functional groups and the width of nanoribbons. As a proof of principle, we considered the model system $\text{H}+\text{NO}_2/\text{OH}-8\text{-ZGNR}$ shown in Figure 3b. By replacing OH groups with H atoms as in $\text{H}+\text{NO}_2/\text{H}-8\text{-ZGNR}$ or by reducing its width to $n = 4$ as in $\text{H}+\text{NO}_2/\text{OH}-4\text{-ZGNR}$, both systems loss the half metallicity and become spin-polarized semiconductors, as shown in Figure 9a,b, respectively.

Conclusions

In conclusion, a systematic theoretical study of edge-decorated ZGNRs is presented. It is predicted that the half-metallicity can be possibly realized in ZGNRs with one edge decorated with the OH functional groups and the opposing edge with either SO_2 or NO_2 functional groups. Reducing the concentration of the SO_2 or NO_2 functional groups along with adding H atoms between them avoid strong steric repulsion between two nearest functional groups while not affecting half-metallicity. Two mechanisms are identified to potentially achieving half-metallicity in ZGNRs. The first is to create a difference in chemical potential between the two edges by decorating one edge with electron-donating groups and another with electron-accepting groups, and the second is to introduce a spin-polarized impurity state at the Fermi level through hybrid modification of one edge with isolated SO_2 groups. A major advantage of the impurity-state mechanism is that the half-metallicity could be achieved in a more flexible fashion, such that the opposing edge (to the SO_2 -decorated edge) of a ZGNR can be decorated by a variety of functional groups (e.g., F, H, or OH) to meet the needs for nanoelectronic applications.

Acknowledgment. We thank Dr. Yi Gao for helpful discussions. This work was supported by grants from ONR (N00014-05-1-0432), NSF (CMMI-0825905), and the Nebraska Research Initiative and by the University of Nebraska Holland Computing Center.

Supporting Information Available: Calculated band structures using three density functionals and deformation densities are collected. This material is available free of charge via the Internet at <http://pubs.acs.org>.

References and Notes

- (1) Novoselov, K. S.; Geim, A. K.; Morozov, S. V.; Jiang, D.; Katsnelson, I. V.; Grigorieva, I. V.; Dubonos, S. V.; Firsov, A. A. *Nature* **2005**, 438, 197.

- (2) Katsnelson, M. L.; Novoselov, K. S.; Geim, A. K. *Nat. Phys.* **2006**, *2*, 620.
- (3) Castro Neto, A. H.; Guinea, F.; Peres, N. M. R. *Phys. World.* **2006**, *19*, 33.
- (4) Zhou, S. Y.; Gwenon, G. H.; Graf, J.; Furdorov, A. V.; Spataru, C. D.; Diehl, R. D.; Kopelevich, Y.; Lee, D. H.; Louie, S. G.; Lanzara, A. *Nat. Phys.* **2006**, *2*, 595.
- (5) Geim, A. K.; Novoselov, K. S. *Nat. Mater.* **2007**, *6*, 183.
- (6) Novoselov, K. S.; Jiang, Z.; Zhang, Y.; Morozov, S. V.; Stormer, H. L.; Zeitler, U.; Maan, J. C.; Boebinger, G. S.; Kim, P.; Geim, A. K. *Science* **2007**, *315*, 1379.
- (7) Zheng, Y.; Ando, T. *Phys. Rev. B* **2002**, *65*, 245420.
- (8) Novoselov, K. S.; Geim, A. K.; Morozov, S. V.; Jiang, D.; Zhang, Y.; Dubonos, S. V.; Firsov, A. A. *Science* **2004**, *306*, 666.
- (9) Fujita, M.; Wakabayashi, K.; Nakada, K.; Kusakabe, K. *J. Phys. Soc. Jpn.* **1996**, *65*, 1920.
- (10) Wakabayashi, K.; Sigrist, M.; Fujita, M. *J. Phys. Soc. Jpn.* **1998**, *67*, 2089.
- (11) Nakada, K.; Fujita, M.; Dresselhaus, G.; Dresselhaus, M. *Phys. Rev. B* **1996**, *54*, 17954.
- (12) Kusakabe, K.; Maruyama, M. *Phys. Rev. B* **2003**, *67*, 092406.
- (13) Lee, H.; Son, Y. W.; Park, N.; Han, S.; Yu, J. *Phys. Rev. B* **2005**, *72*, 174431.
- (14) Rudberg, E.; Salek, P.; Luo, Y. *Nano Lett.* **2007**, *7*, 2211.
- (15) Pisani, L.; Chan, J. A.; Montanari, B.; Harrison, N. M. *Phys. Rev. B* **2007**, *75*, 064418.
- (16) Hod, O.; Barone, V.; Scuseria, G. E. *Phys. Rev. B* **2008**, *77*, 035411.
- (17) Hod, O.; Peralta, J. E.; Scuseria, G. E. *Phys. Rev. B* **2007**, *76*, 233401.
- (18) Hod, O.; Barone, V.; Peralta, J.; Scuseria, G. *Nano Lett.* **2007**, *7*, 2295.
- (19) Barone, V.; Hod, O.; Scuseria, G. *Nano Lett.* **2006**, *6*, 2748.
- (20) Son, Y. W.; Cohen, M. L.; Louie, S. G. *Phys. Rev. Lett.* **2006**, *97*, 216803.
- (21) Groot, R. A.; Mueller, F. M.; Engen, P. G.; Buschow, K. H. J. *Phys. Rev. Lett.* **1983**, *50*, 2024.
- (22) Prinz, G. A. *Science* **1998**, *282*, 1660.
- (23) Ziese, M. *Rep. Prog. Phys.* **2002**, *65*, 143.
- (24) Son, Y. W.; Cohen, M. L.; Louie, S. G. *Nature* **2006**, *444*, 347.
- (25) (a) Kan, E. J.; Li, Z.; Yang, J. L.; Hou, J. G. *Appl. Phys. Lett.* **2007**, *91*, 243116. (b) Kan, E. J.; Li, Z.; Yang, J. L.; Hou, J. G. *J. Am. Chem. Soc.* **2008**, *130*, 4224.
- (26) Li, Y.; Zhou, Z.; Shen, P.; Chen, Z. F. *ACS Nano* **2009**, *3*, 1952.
- (27) Wu, M.; Wu, X.; Gao, Y.; Zeng, X. C. *Appl. Phys. Lett.* **2009**, *94*, 22311.
- (28) Kresse, G.; Hafner, J. *Phys. Rev. B* **1993**, *47*, 558.
- (29) Kresse, G.; Furthmuller, J. *Phys. Rev. B* **1996**, *54*, 11169.
- (30) Kresse, G.; Joubert, D. *Phys. Rev. B* **1999**, *59*, 1758.
- (31) Perdew, J. P.; Burke, K.; Ernzerhof, M. *Phys. Rev. Lett.* **1996**, *77*, 3865.
- (32) Monkhorst, H. J.; Pack, J. D. *Phys. Rev. B* **1976**, *13*, 5188.
- (33) Heyed, J.; Scuseria, G. E. *J. Chem. Phys.* **2004**, *121*, 1187.
- (34) Heyed, J.; Peralta, J. E.; Scuseria, G. E. *J. Chem. Phys.* **2005**, *123*, 174101.
- (35) Yang, L.; Cohen, M.; Louie, S. *Nano Lett.* **2007**, *7*, 3112.
- (36) Prezzi, D.; Varsano, D.; Ruini, A.; Marini, A.; Molinari, E. *Phys. Rev. B* **2008**, *77*, 041404.
- (37) Ritter, K. A.; Lyding, J. W. *Nat. Mater.* **2009**, *8*, 235.

JP100027W